Chapter 11

Optimization of Fuzzy Logic Controllers by Particle Swarm Optimization to Increase the Lifetime in Power Electronic Stages

Pedro Ponce, Luis Arturo Soriano,
Arturo Molina and Manuel Garcia

Additional information is available at the end of the chapter

http://dx.doi.org/10.5772/intechopen.79212

Abstract

In recent years, brushless direct current motor (BLDCM) applications have been increased due to their advantages as low size, mechanical torque, high-speed range, to mention some. The BLDCM control is required to operate at high frequency, high temperature, large voltage, and quick changes of current; as a result of this kind of operation, the power drive lifetime is affected. The power drives commonly utilized insulated gate bipolar transistors (IGBTs) and metal oxide semiconductor field effect transistors (MOSFETs), which present power losses, on-state losses, and switching losses caused by temperature oscillations. Hence, the power losses are related to the command signals generated by the controller. In this sense, the BLDC motor drive controller design, frequently, does not take into account the power losses and the temperature oscillations, which cause the IGBT lifetime decrease or premature fail. In this chapter, a brushless DC motor drive is designed based on a fuzzy controller tuned with the particle swarm optimization algorithm, where the temperature oscillations and speed set points are considered in order to increase IGBT module lifetime. The validation of the proposed fuzzy-PSO controller is carried out by the co-simulation between LabVIEW™ and Multisim™ and finally analysis and conclusion of the work.

Keywords: power electronics lifetime, speed controller, fuzzy logic, PSO, BLDCM

1. Introduction

In this chapter, a design of a BLDCM speed control based and tuned by particle swarm optimization is presented; this proposal control considers two objectives, the first one is

the speed set point and the second one is the power electronic lifetime. The BLDC motor covers a wide range of applications in several fields as the robotic systems, aerospace industry, medical industry, automotive industry, and electronic devices [8, 17, 25, 32]. Their structure of control is integrated by BLDC motor stage, power drive stage, and sensor stage. The power drive is integrated by semiconductors as IGBTs and MOSFETs, these semiconductors frequently work under high thermal stress to reach the mechanical reference of speed, and in some cases, after a certain period of operation, they are damaged due to the generation of command signals by the speed controller [7, 9, 12, 23, 34, 35]. There are several methods to predict and evaluate the lifetime of power electronics devices [34], the manufactures develop these studies as an estimation of certain conditions and operation features, but in some applications, these conditions are not always the same and change according to the control objective, which affects the power electronics lifetime used. For these reason, it is important that the controller design not only considers the mechanical references such as position and velocity in the case of BLDCM, as well as the lifetime of semiconductors [10, 22, 23, 24, 33, 34, 35]. Hence, a great effort for predicting and improving the lifetime in semiconductors has been pushing to develop new control algorithms that help to improve the conditions in the semiconductor [16]. In this chapter, the designed controller uses an optimization process based on an objective function that takes into account the temperature of the power electronic stages in order to increase their lifetime, and tracking motor speed reference [1, 10]. Thus, PSO algorithm has been implemented to optimize the controller proposed as in [13, 18, 21, 27, 30], due to its few parameters that need to be tuned and its easy implementation. Finally, the proposed controller in BLDCM is validated through co-simulation, which helps to combine two or more specialized programs utilizing advanced models and avoiding implementation problems between the control systems and power electronics stage [11, 14, 15].

2. Structure and drive mode of BLDC motor

2.1. Types of BLDCM drives

The BLDC motor drive employs a permanent magnet alternating current; the stator windings are commonly star connection, when voltage source is applied between any two terminals, the current flows between two phases, leaving one of the three without energy, and as a result, only one current at a time needs to be controlled. This kind of operation is known as back electromotive force (EMF) and **Figure 1** shows the waveform in the BLDC motor with two phases active.

According to their physical position, the output is related to 60° or 120° phase shift to each other. To drive the windings, a sequence of commutation is necessary; this kind of operation is commonly called "six-step commutation." The trapezoidal waveform is due to the rotor revolving in a counterclockwise direction, for example, to phase A, after the 120° rotation to the top conductor of phase.

The motor position must be measured by three Hall effect sensors (A, B, and C) so a voltage is sent to the specific coils to control the speed and position of the brushless motor [3, 25]. A standard circuit to drive BLDCM in Multisim™ program is shown in **Figure 2**.

http://dx.doi.org/10.5772/intechopen.79212

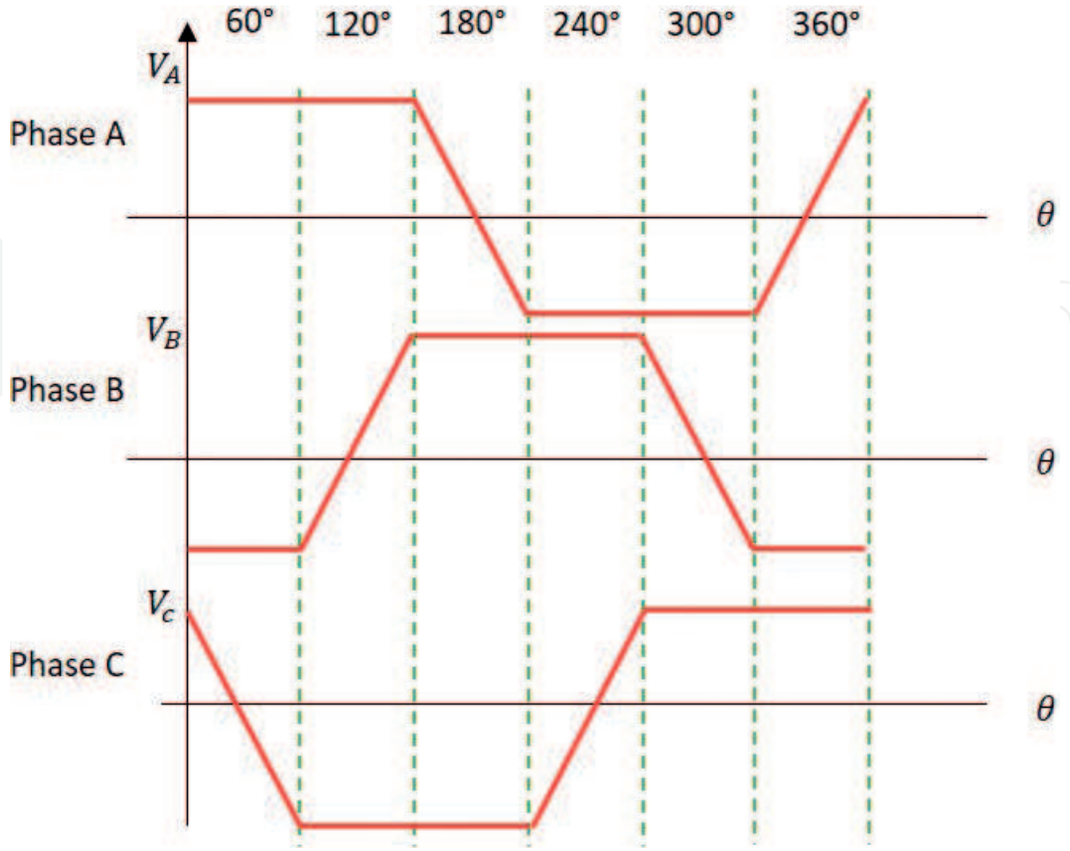

Figure 1. Trapezoidal EMF.

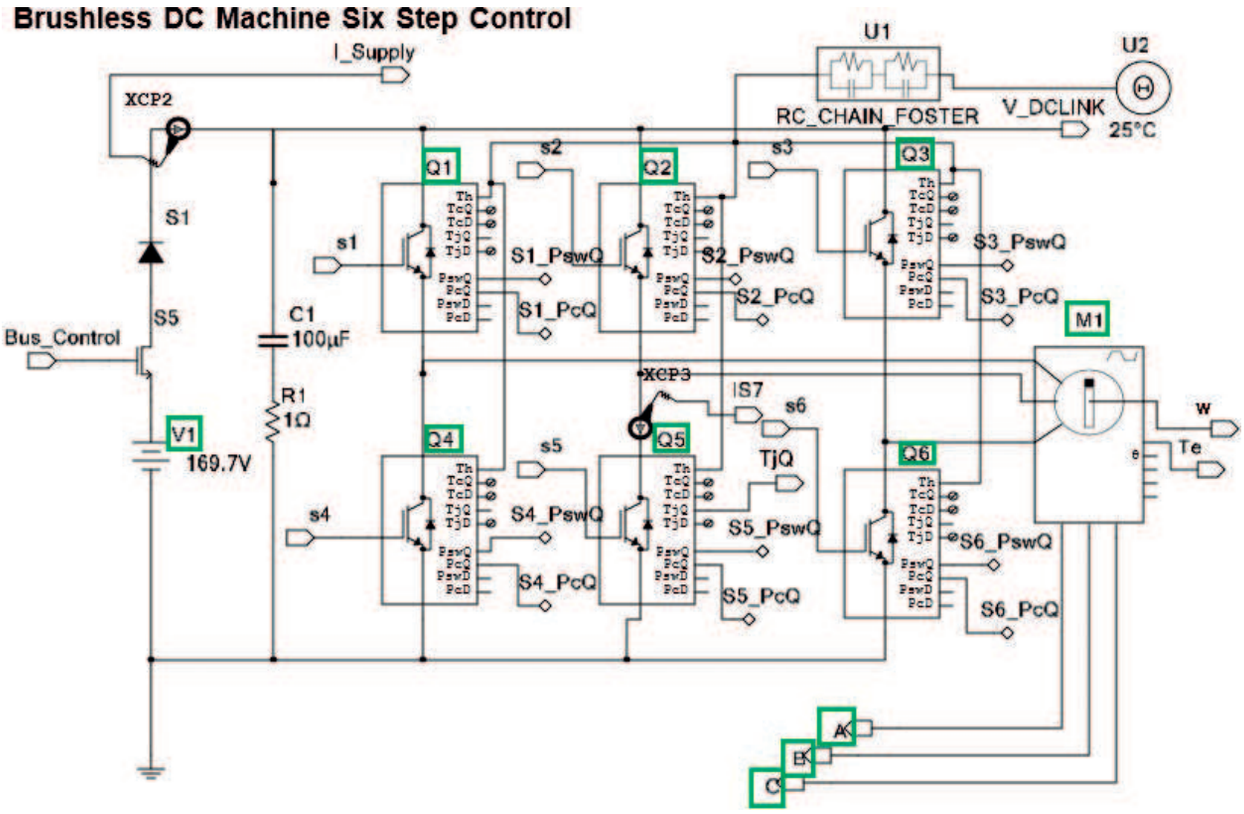

Figure 2. BLDCM drive in Multisim™ for co-simulation.

2.2. States space model

According to [25], the BLDCM can be represented by Eq. (1) where R is the stator resistance per phase, i_{as}, i_{bs}, and, i_{cs} are the stator phase current, and e_{as}, e_{bs}, and e_{cs} are the rotating back-EMF that are produced by the winding flux linkage caused by rotating rotor.

$$\begin{bmatrix} u_{as} \\ u_{bs} \\ u_{cs} \end{bmatrix} = R \begin{bmatrix} 100 \\ 010 \\ 001 \end{bmatrix} \begin{bmatrix} i_{as} \\ i_{bs} \\ i_{cs} \end{bmatrix} + (L-M) \begin{bmatrix} 100 \\ 010 \\ 001 \end{bmatrix} \frac{d}{dt} \begin{bmatrix} i_a \\ i_b \\ i_c \end{bmatrix} + \begin{bmatrix} e_{as} \\ e_{bs} \\ e_{cs} \end{bmatrix} \tag{1}$$

The induced EMF is given by the Eq. (2)

$$\begin{aligned} e_{as} &= \omega \psi_m f_{as}(\theta) \\ e_{bs} &= \omega \psi_m f_{bs}(\theta) \\ e_{cs} &= \omega \psi_m f_{cs}(\theta) \end{aligned} \tag{2}$$

where $f_{as}(\theta)$, $f_{bs} = f_{as}(\theta - 2\pi/3)$ and $f_{cs} = f_{as}(\theta + 2\pi/3)$ are the back-EMF waveform function of phase, respectively. ψ_m is the maximum value of PM; the flux linkage of each winding as $\psi_m = 2NSBm$. On the other hand, the dynamic features of BLCDM are expressed in state equations as shown in Eq. (3):

$$\begin{bmatrix} \dot{i_{as}} \\ \dot{i_{bs}} \\ \dot{i_{cs}} \\ \dot{\omega_m} \\ \dot{\theta_r} \end{bmatrix} = \begin{bmatrix} -\frac{R_s}{L_1} & 0 & 0 & -\frac{\psi_m}{J} f_{as(\theta_r)} \\ 0 & -\frac{R_s}{L_1} & 0 & -\frac{\psi_m}{J} f_{bs(\theta_r)} \\ 0 & 0 & -\frac{R_s}{L_1} & -\frac{\psi_m}{J} f_{cs(\theta_r)} \\ \frac{\psi_m}{J} f_{as(\theta_r)} & \frac{\psi_m}{J} f_{bs(\theta_r)} & \frac{\psi_m}{J} f_{cs(\theta_r)} & -\frac{B}{J} \end{bmatrix} \begin{bmatrix} i_{as} \\ i_{bs} \\ i_{cs} \\ \omega_m \\ \theta_r \end{bmatrix} + \begin{bmatrix} \frac{1}{\mathrm{L-M}} & 0 & 0 & 0 \\ 0 & \frac{1}{\mathrm{L-M}} & 0 & 0 \\ 0 & 0 & \frac{1}{\mathrm{L-M}} & 0 \\ 0 & 0 & 0 & \frac{1}{J} \end{bmatrix} \begin{bmatrix} v_{as} \\ v_{bs} \\ v_{cs} \\ T_l \end{bmatrix} \tag{3}$$

where windings are symmetrical, the self-inductance will be equal, and so as the mutual inductance, $L_{as} = L_{bs} = L_{cs} = L \; and \; L_{ab} = L_{bc} = L_{ca} = M$. The electromagnetic torque is given in Eq. (4):

$$T_e = \psi_m \left[f_{as}(\theta_r) i_{as} + f_{bs}(\theta_r) i_{bs} + f_{cs}(\theta_r) i_{cs} \right] (N.m) \tag{4}$$

and, the complete model of the electromechanical system is described by Eq. (5):

$$T_e - T_l = J \, \dot{\omega}_m + B \omega_m \tag{5}$$

where T_l is the load torque, J is the rotor moment of inertia, and B is the viscous coefficient.

http://dx.doi.org/10.5772/intechopen.79212

3. Power losses

3.1. Semiconductor losses

Power losses can be classified as on-state losses and switching losses. The IGBT power losses in on-state are calculated by Eq. (6):

$$P_{CT} = u_{CEO} * I_{Cav} + r_c I_{Crms}^2 \tag{6}$$

and the diode power losses in on-state are calculated by Eq. (7):

$$P_{CD} = u_{DO} * I_{Dav} + r_D I_{Drms}^2 \tag{7}$$

These can also be estimated using datasheet information of **Figure 3**. On the other hand, the IGBT energy losses in turn-on are given by Eq. (8):

$$E_{onT} = \int_{ton} (u_{CEO} * i_C(t)) dt \tag{8}$$

and, the energy losses in turn-off are given by Eq. (9):

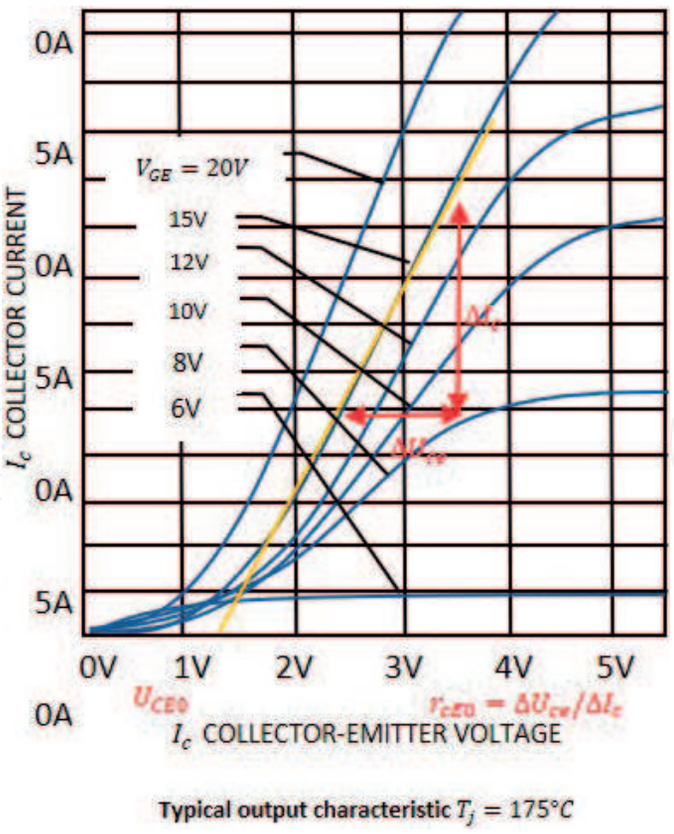

Figure 3. The u_{CEO} and r_c ($r_c = \Delta U_{ce}/\Delta I_c$) values of datasheet diagram.

$$E_{offT} = \int_{toff} (u_{CEO} * i_C(t))dt \tag{9}$$

On the other hand, the diode energy losses in turn-on are mostly presented when the reverse-recovery energy occurs, and they are given by:

$$E_{onD} = \int_{toff} (u_D(t) * i_F(t))dt \tag{10}$$

The switch-off losses in the diode are commonly neglected $E_{offD} \approx 0$. In consequence, the switching losses in the IGBT are calculated in Eq. (11) as:

$$P_{swT} = \left(E_{onT} + E_{offT}\right) * F_{sw} \tag{11}$$

In the case of a diode, they are given as the product of switching energies and the switching frequency F_{sw} as shown in Eq. (12).

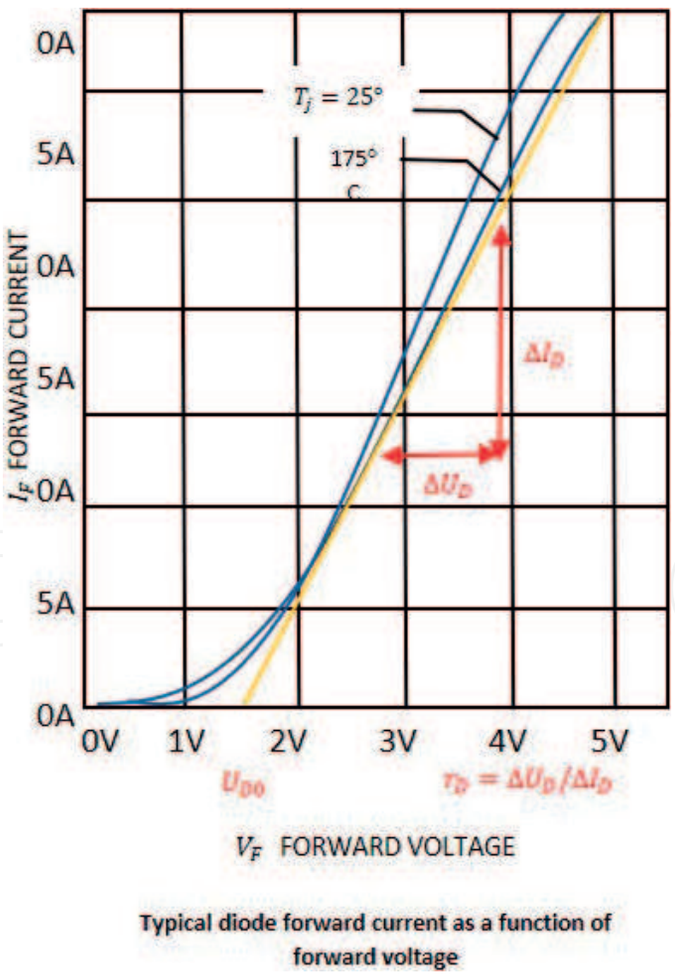

Figure 4. The u_{DO} and r_D ($r_d = \Delta U_{ce}/\Delta I_c$) values of datasheet diagram.

http://dx.doi.org/10.5772/intechopen.79212

$$P_{swD} = \left(E_{onD} + E_{offD}\right) * (F_{sw}) \approx E_{onD} * (F_{sw}) \tag{12}$$

Finally, the total losses are calculated by Eq. (13).

$$W = P_{CT} + P_{swT} + P_{CD} + P_{swD} \tag{13}$$

Besides, the IGBT and diode switching losses can be estimated from characteristic curve provided by datasheet of manufactures as shown in **Figures 3**, **4** and **5**, respectively [5]. Using the equivalent circuit of **Figure 6(a)**, where W is a module power loss, T_j is the junction temperature IGBT chip, T_f is the heat sink temperature, T_c is the module case temperature, T_a is the ambient temperature, $R_{th(j-c)}$ is the thermal resistance between case and heat sink, $R_{th(c-f)}$ is the contact thermal resistance between case and heat sink, and $R_{th(f-a)}$ is the thermal resistance between heat sink and ambient air. The junction temperature T_j can be calculated using the thermal Eq. (14), according to [1, 10].

$$T_j = W * (Rth(j-c) + Rth(c-f) + Rth(f-a)) + Ta \tag{14}$$

Modeling of commutation and conduction losses as well as the temperature profiles on IGBT junction is done by electrothermic networks considering averages on a modulation period as shown in **Figure 6(b)**.

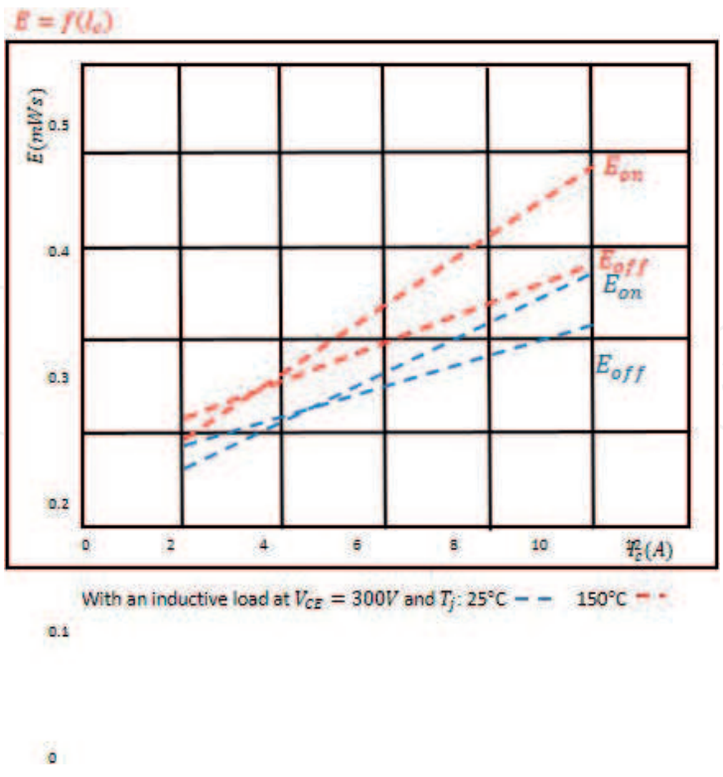

Figure 5. Switching energy losses as a function of collector current.

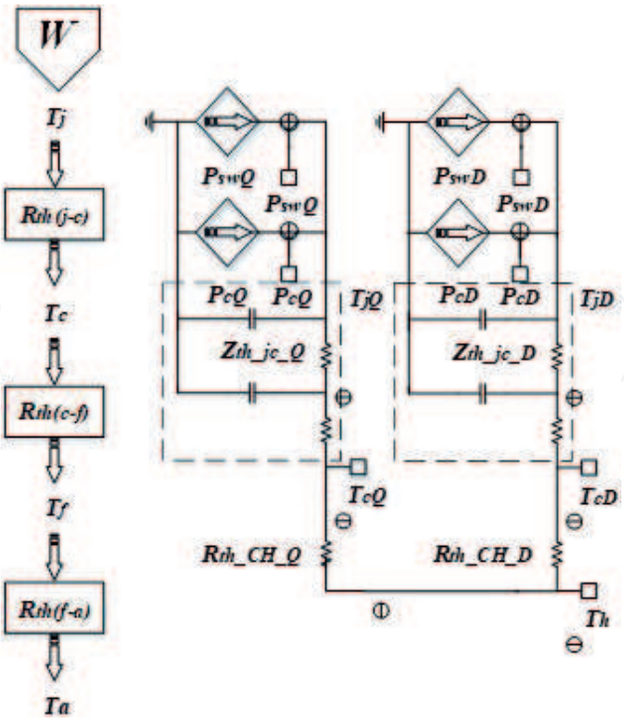

Figure 6. (a) Thermal resistance equivalent circuit, (b) electrothermal model.

4. Power cycle life

The power cycle life can be calculated from the power cycle capability curve that shows the relation between the temperature change ΔT_j and the number cycles. An example of the temperature changes is shown in **Figure 7**.

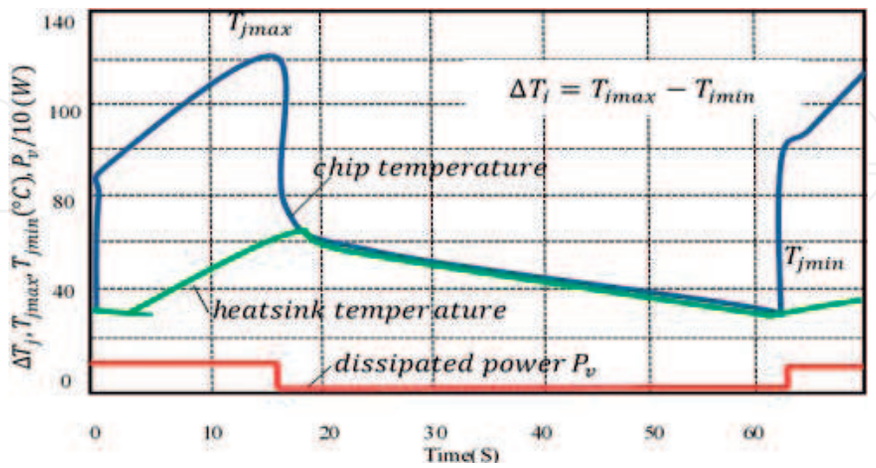

Figure 7. Pattern diagram flow current of ΔT_j power cycle and temperature change.

http://dx.doi.org/10.5772/intechopen.79212

During the ΔT_j power cycle tests, the junction temperature goes up and down in a short time cycle; as a consequence, the temperature difference between silicon and bonding wire results in thermal stress. The ΔT_j power cycle lifetime is mainly limited by the aluminum bonding wire joints. **Figure 8** shows the power cycle capability curve of the IGBT module to $\Delta T_{jmin} = 25^{\circ} C$ and to $\Delta T_{jmax} = 150^{\circ} C$ according to [5].

On the other hand, the cycles before failure (CBF) can be calculated by Eq. (15), according to [28, 29].

$$CBF = 541162959016419 * \Delta T^{-5.12121} \tag{15}$$

where $\Delta\ T = P_t Z_{th}$, $P_t = I_{rms}^2 R_{on}$, and $Z_{th} = 2.3354 F_r^{-0.165}$, and the time before failure (TBF) can be calculate in years by Eq. (16).

$$TBF = \frac{CF}{Fr} * 60 * 24 * 265 \ years \tag{16}$$

where F_r is the frequency of the thermal oscillations [5, 29]. **Table 2** shows the parameters of IGBTs, which are considered in Multisim co-simulation; these parameters are obtained from datasheet of IGBT 10-0B066PA00Sb-M992F0 [24].

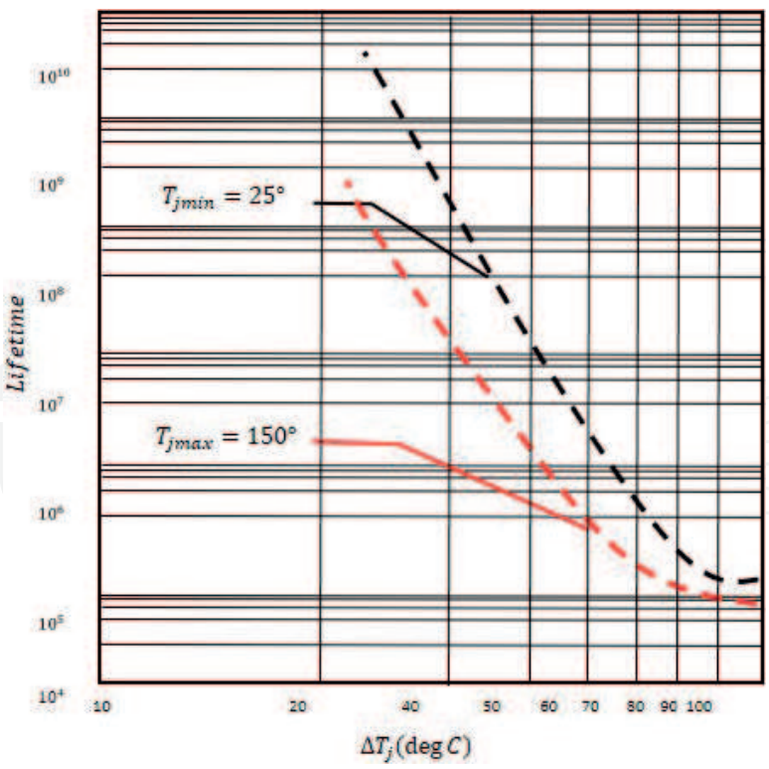

Figure 8. Power cycling lifetime curve.

5. Fuzzy logic controller

The fuzzy logic was proposed in [26] as a class of fuzzy sets with a continuum grade of membership; hence, a useful methodology to design fuzzy logic controllers is based on a linguistic phase plane [19, 20] as shown in **Figure 9**, where the error $e(t)$, change of error $\dot{e}(t)$, and the variation of current i_c are considered as membership functions in the fuzzification stage.

$$e(t) = e_c + e_t \tag{17}$$

$$\dot{e}(t) = \frac{\Delta e(t)}{\Delta t} = e(t) - e(t-1) \tag{18}$$

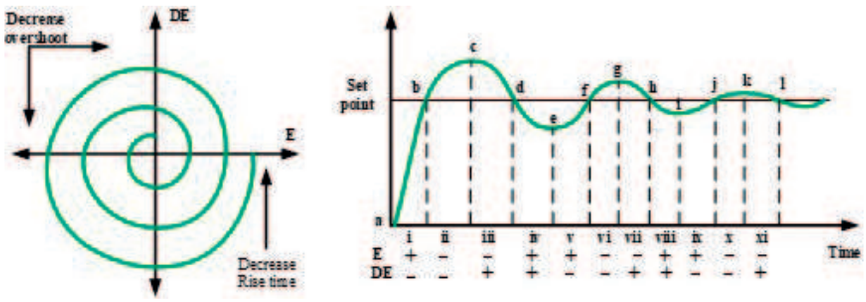

Figure 9. Linguistic phase plane.

Rules	Values			Reference point
	e	$\dot{e}$	i_c	
1	P	Z	P	a,e,i
2	N	N	Z	b,f,j
3	N	Z	N	c,g,k
4	P	P	Z	d,h,l
5	Z	Z	Z	sp
6	P	N	P	i(rt)v
7	N	N	N	ii(os) vi
8	N	P	N	iii,vii
9	P	P	P	iv,viii
10	Z	N	P	ix
11	Z	P	N	xi

Note: The meaning of symbols is as follows, N: negative, Z: zero, P: positive, e: error, $\dot{e}$: error derivative, i_c: output, sp: set point, rt: rise time, os: overshot.

Table 1. Fuzzy control rules for **Figure 12**.

http://dx.doi.org/10.5772/intechopen.79212

Thus, Eq. (17) is defined as the sum of control error (e_c) and error of temperature (e_t), where e_c is defined as the difference of the desired speed e_d and the real speed e_r; on the other hand, e_t is defined as $e_t = e_{td} - e_{tr}$, where e_{td} is the desired temperature and e_{tr} is the real temperature.

The design of membership functions is according to Mamdani method; the knowledge base can be expressed as if-then statements to design a rules base, which is shown in **Table 1**. At last, the defuzzification stage gets a crisp value from the rule evaluation stage. Hence, the method of the center of gravity is used to compute the crisp value and is given by Eq. (19).

$$z^* = \frac{\int \mu_B(z) \cdot z dz}{\int \mu_B(z) dz} \tag{19}$$

So that, the fuzzy control design is carried out by means of the linguistic plane and the rules presented in **Table 1**. Thus, the controller with small/big rise time as well as small/big overshoot is possible.

6. Particle swarm optimization

Particle swarm optimization (PSO) was developed by [4]; this method is based on the behavior and movement of bird flocks looking for targets; this algorithm was developed to optimize nonlinear and multidimensional functions as in [13, 18, 27, 30, 31]. PSO algorithm needs to initialize the population in a random manner; each particle has a position $x_i(t)$ and velocity $v_i(t)$ with respect to target; then in main loop stage, the $x_i(t)$ and $v_i(t)$ update each iteration; this information is called best local position $P_i(t)$; on the other hand, between all population, there exists a particle that is more closest with respect to the target and it is called global best $g(t)$. Additionally, the position and velocity update are defined by:

$$v_{ij}(k+1) = \omega v_{ij}(k) + r_{1j} C_1 \left(\mathrm{P}_{ij}(k) - x_{ij}(k) \right) + r_{2j} C_2 \left(g_j(k) - x_{ij}(k) \right) \tag{20}$$

$$x_{ij}(k+1) = x_{ij}(k) + v_{ij}(k+1) \tag{21}$$

where

- $i = 1, 2, \ldots, N$, and N is the size of population;
- $j = 1, 2, \ldots, D$, and D is the number of dimensions;
- $k = 1, 2, \ldots, iter$, and $iter$ is the maximum iteration number;
- $x_{ij}(k)$ is the position of particle i, dimension j at iteration k;
- $v_{ij}(k)$ is the velocity of particle i, dimension j at iteration k;
- $P_{ij}(k)$ is the local best position of particle i, dimension j at iteration k;
- $g_j(k)$ is the global best;
- ω is an inertia factor;

- C is an acceleration constant; and
- r_1, r_2 are the independent random numbers, uniformly distributed in $(0, 1)$.

Thus, the primary objective is to find a minimal global value from the cost function to be minimized as it is shown in the next pseudocode [31].

Step 1. Initialization.

For each particle of population N,

1. Initialize the position of each particle.
2. Initialize $P_{ij}(k)$.
3. Initialize $g_j(k)$.
4. Initialize $v_{ij}(k)$.

Step 2. Repeat until the criterion is satisfied.

For each particle of population N,

1. Set random numbers to r_{1j} and r_{2j}.
2. Update its velocity with Eq. (20).
3. Update its position with Eq. (21).
4. If $x_{ij}(k) < P_{ij}(k)$, then
   a. Update the best local position.
   b. If $P_{ij}(k) < g_j(k)$, then update the best global position $\mathrm{g}(k)$.

Step 3. Get the best solution $\mathrm{g}(k)$.

7. Design of fuzzy-PSO controller

The design of controller considers two objectives, the first one reaches the desired motor speed, and the second one is the increase of the semiconductor lifetime. The design of fuzzy-PSO controller to the speed control of BLDCM is based on the diagram shown in **Figure 11**, where μ_d is the desired speed and temperature, μ_t is the temperature sensed, and μ_c is the speed sensed. Furthermore, one of the leading features is the definition of objective function; this is considered as the sum of error of temperature e_t and error of speed e_c, which is given by Eq. (22).

$$f_c = e_c + e_t \tag{22}$$

where e_t is the difference between the desired temperature and the operating temperature; on the other hand, e_c is the difference between the desired speed and the real speed. In optimization

http://dx.doi.org/10.5772/intechopen.79212

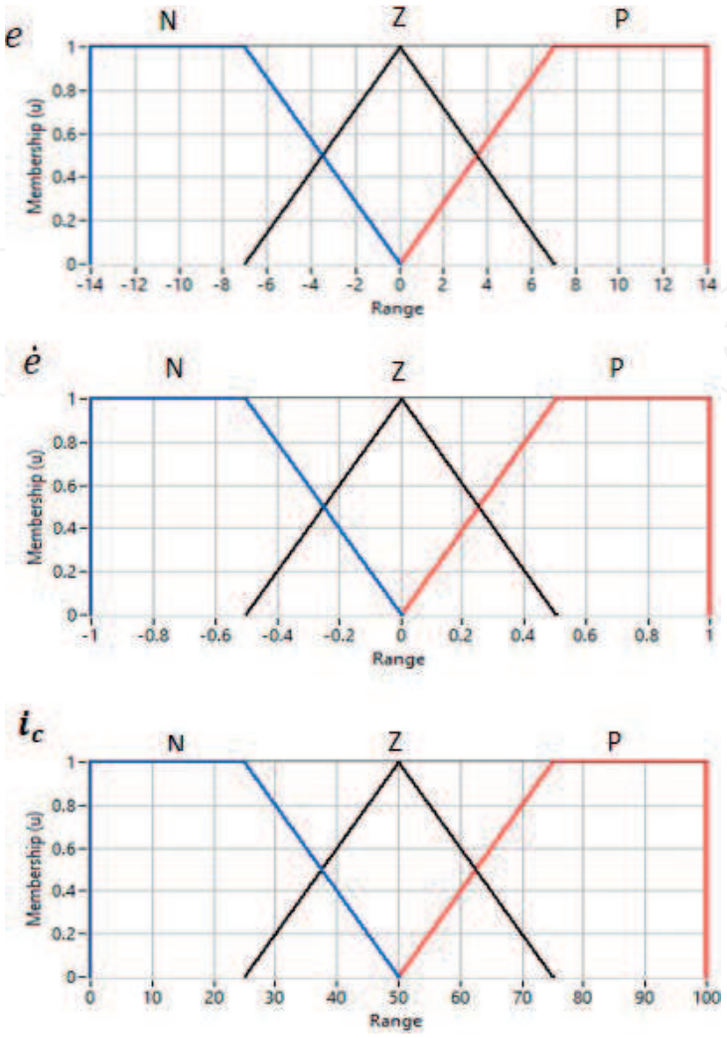

Figure 10. Diagram of fuzzy-PSO control.

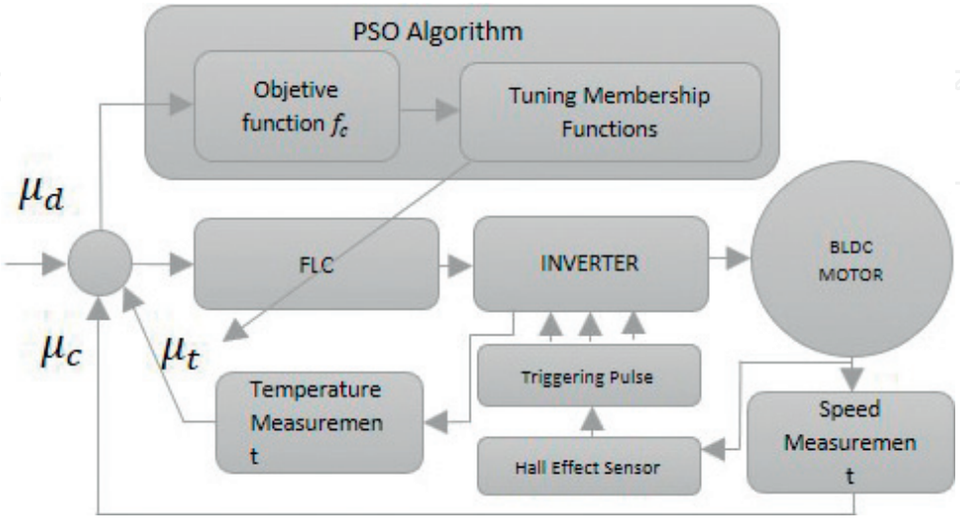

Figure 11. Input-output membership functions where e: error, $\dot{e}$: error derivative, and i_c: output.

IGBT 10-0B066PA00Sb-M992F09		
Parameter	Value	Unit
V_{CE}	600	mH
$R_{CE(ON)}$	0.1	Ω
I_C	8–6	Vs/rad
T_J, junction temperature	80 to 175	Nm/A
R_{J-S} thermal resistance junction to sink	3.50	K/W
BLDC motor		
Stator inductance	0.15	mH
Stator resistance	0.6	Ω
Velocity constant	0.03	Vs/rad
Torque constant	0.03	Nm/A
Number of poles	0.03	
Parameter of IGBT in co-simulation Multisim™		
IGBT control threshold	0.5	V
IGBT on resistance	0.1 meg	Ω
IGBT off resistance	10	Ω
IGBT forward voltage drop	0.7	V
Diode on resistance	1 m	Ω
Diode off resistance	10 meg	Ω
Number of switches in parallel	1	

Table 2. Experiment settings.

process, Eq. (22) is defined as the cost function to be minimized, and each membership functions proposed in **Figure 10** are considered as a decision variable; finally, the mechanical capacity of BLDC and thermal capacity of IGBT shown in **Table 2** are the constraints of the controller optimization.

8. Co-simulation design

The experimental frame is a set of assumptions to obtain the behavior trace and compare it with a real world, which is carried out by co-simulation in order to analyze its dynamic response during a specific period of time [6]. Hence, co-simulation helps to validate how it works under specific assumptions [2, 6]. The problem solution of speed control and lifetime of power electronic components is developed with co-simulation tool of Labview™ and Multisim™, where the BLDCM, the Hall effect sensors, and the six steps are simulated in Multisim™ and the

http://dx.doi.org/10.5772/intechopen.79212

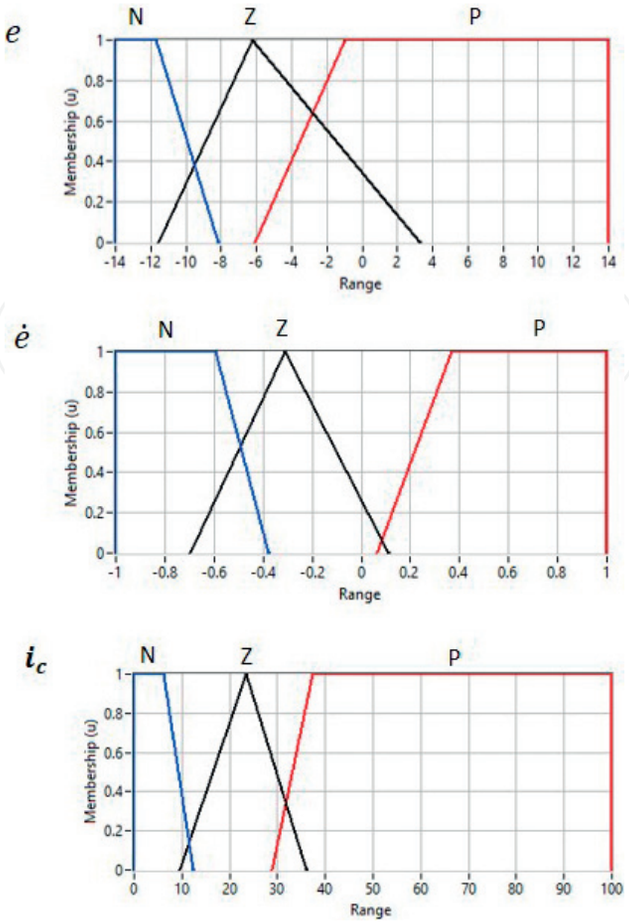

Figure 12. BLDCM speed response.

parameter design of the BLDCM, the six IGBT 10-0B066PA00Sb-M992F09 [24], and the six-steps inverter are shown in **Table 2**.

The proposal control is developed in Labview™ software and its response is shown in **Figure 14**, and the PID and fuzzy control are developed with control design and simulation module and fuzzy logic toolkit [19]; moreover, PSO algorithm is also developed in Labview™, and their parameters are shown in **Table 3**.

Finally, the primary purpose of co-simulation is to analyze the complete behavior of the electric drive with the proposed control.

Parameter	Values
Population size	30
Social rate (c_1)	0.005
Cognitive rate (c_2)	0.002
Inertia factor (W)	0.002

Table 3. Parameters of PSO.

9. Discussion and results

The proposed control considers two control objectives, the first one is to track the speed reference and the second one is to keep the desired temperature to increase the lifetime of the IGBTs. Furthermore, the fuzzy-PSO trade-off was tested with PID and fuzzy controllers in co-simulation program, which were evaluated under 25, 30, 35, 40, 60, 80, and 100°C as a temperature desired, 10 and 5 m/s as the reference speed, respectively. As a result, the PID controller response reaches set point of speed in a short time, but it does not present an improvement in the temperature of semiconductors. The fuzzy logic controller improves the response when the desired temperature values are at 40° and 60° and fuzzy-PSO controller presents the best response in order to accomplish the control objective because they reduce the overshoot of current when it reaches the temperature and reference speed. **Figures 13** and **14** show the response of controllers, and **Figure 12** shows the final membership function adaptation of fuzzy-PSO controller.

Table 4 shows the mean square error (MSE) of each controller under different desired temperatures, where the MSE of the fuzzy-PSO response shows good performance. To compare the proposed control response with the traditional estimation, the cycles before failure (*CBF*) given by Eq. (15) was computed to take into account the maximum temperature T_{jmax}, the change of temperature, $\Delta T = T_{jmax} - T_f$, and the IGBT datasheet.

Table 5 shows the calculation of TBF of the PID, fuzzy, and fuzzy-PSO controllers according to Eq. (16), and **Figure 15** shows the behavior of the TBF versus temperature, where the fuzzy-PSO controller reaches a longer lifetime.

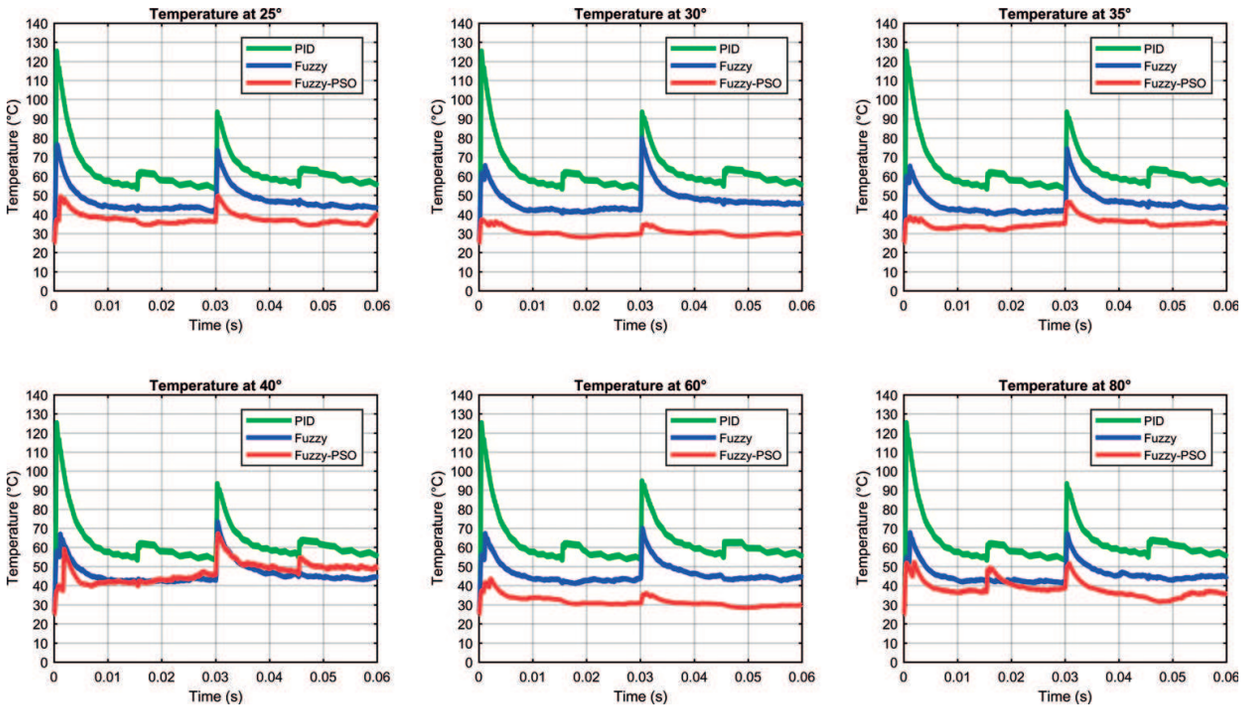

Figure 13. PID, fuzzy, and fuzzy-PSO controllers under different temperatures.

http://dx.doi.org/10.5772/intechopen.79212

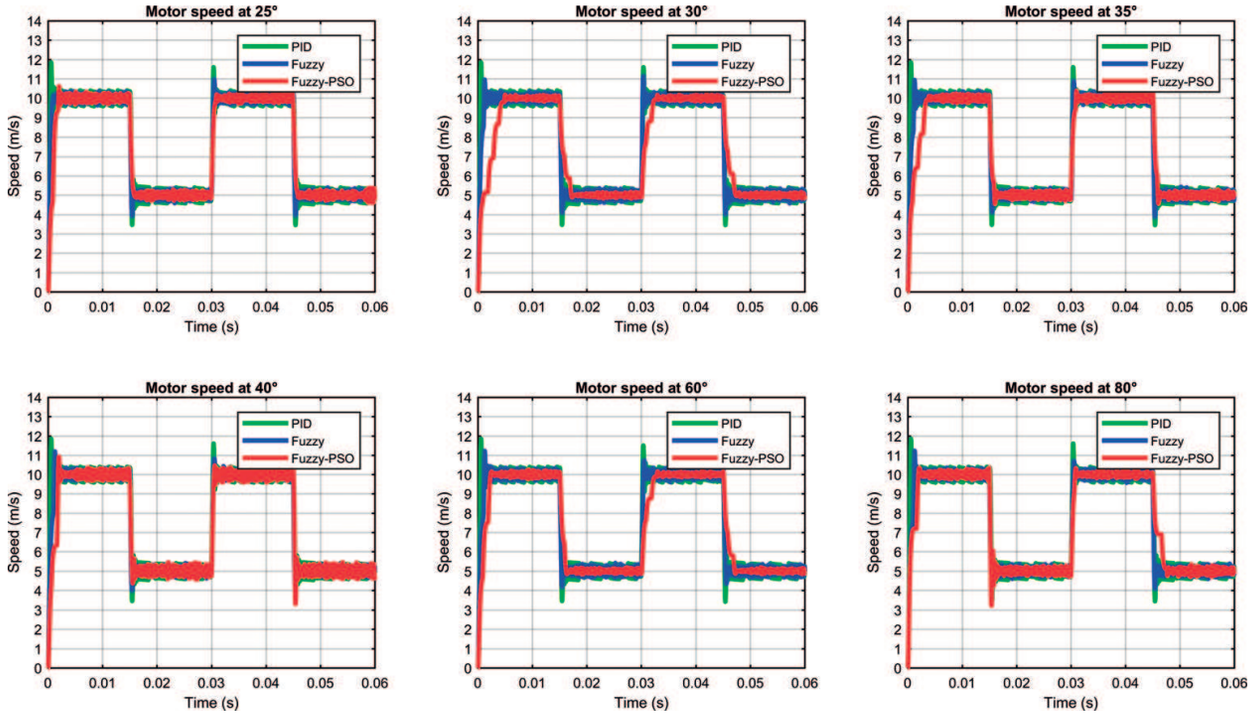

Figure 14. Tuning the input and output membership function parameters by means of the PSO.

MSE/T	25°	30°	35°	40°	60°	80°	100°
PID	61.8	60.8	60.8	60.8	60.8	60.8	60.8
Fuzzy	44.4	44.9	44.5	33.2	39.0	43.7	44.5
Fuzzy-PSO	39.6	37.5	43.7	42.4	52.5	44.0	45.1

Table 4. MSE of controllers.

Temperature	TBF (in years)	Temperature	TBF (in years)
°C	PID	°C	PID
25	0.004105201	25	0.004105201
30	0.005355432	30	0.005355432
35	0.005355432	35	0.005355432
40	0.00535696	40	0.00535696
60	0.00535696	60	0.00535696
80	0.00535696	80	0.00535696
100	0.00535696	100	0.00535696

Table 5. TBF of the controllers.

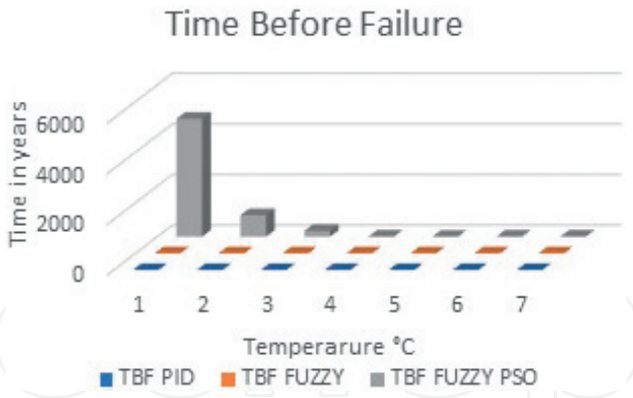

Figure 15. The behavior of TBF versus temperature in years.

10. Conclusions

In this chapter, a control design that takes into account the power electronics lifetime stage and the speed set point for BLDCM is presented. The objective function of optimization is integrated with the error of power stage temperature and the error of BLDCM speed. A voltage source inverter with six IGBT to drive the BLDCM is considered as power stage, where the current temperature in the power electronic stage, reference temperature, current motor speed, and reference motor speed are considered in the controller design. The PID controller, fuzzy logic controller, and fuzzy-PSO controller were designed and validated by NI Labview™ and Multisim™ co-simulation software. As a result, the fuzzy-PSO controller obtains a good response that increases the lifetime and reaches the set point desired due to the time that it takes to reach the desired speed increases but it reduces the overshoot of current during the transition time which produces minimal stress and degradation of the power electronic components.

Acknowledgements

This research is a product of the Project 266632 "Laboratorio Binacional para la Gestión Inteligente de la Sustentabilidad Energética y la Formación Tecnológica" ["Bi-National Laboratory on Smart Sustainable Energy Management and Technology Training"], funded by the CONACYT SENER Fund for Energy Sustainability (Agreement: S0019201401).

Author details

Pedro Ponce[1]*, Luis Arturo Soriano[1], Arturo Molina[1] and Manuel Garcia[2]

*Address all correspondence to: pedro.ponce@itesm.mx

1 Escuela de Ingeniería y Ciencias, Tecnologico de Monterrey, Mexico City, Mexico

2 Escuela Superior de Ingeniería Mecánica y Eléctrica, Instituto Politécnico Nacional, México City, México

References

[1] Bayerer R, Herrmann T, Licht T, Lutz J, Feller M. Model for power cycling lifetime of IGBT modules—Various factors influencing lifetime. In: Integrated Power Systems (CIPS), editor. 5th International Conference on Integrated Power Electronics Systems; March 11–13, 2008; Nuremberg, Germany: VDE; 2008. pp. 1-6

[2] Cellier FE, Kofman, editors. Continuous System Simulation. 1st ed. New York: Springer-Verlag New York, Inc; 2006. 639p

[3] Chau KT, editor. Electric Vehicle Machines and Drives: Design, Analysis and Application. 1st ed. Singapore: John Wiley & Sons, Singapore Pte. Ltd; 2015. 375p. DOI: 10.1002/9781118752555

[4] Eberhart R, Kennedy. A new optimizer using particle swarm theory. In: Micro Machine and Human Science, editor. Proceedings of the Sixth International Symposium on Micro Machine and Human Science; October 4–6, 1995; Nagoya, Japan, Japan: IEEE; 1995. pp. 39-43. DOI: 10.1109/MHS.1995.494215

[5] Fuji Electric. www.fujielectric.com. Fuji IGBT Modules Application Manual [Internet]. 2013 [Updated: January, 2017]. Available from: www.fujielectric.com/products/semiconductor/model/igbt/application/box/doc/pdf/REH984e/REH984e.pdf

[6] Gomes C, Thule C, Broman D, Larsen PG, Vangheluwe H. Co-simulation: State of the art. Cornell University Library. 2017. arXiv preprint arXiv:1702.00686

[7] Gopi Reddy LR, Tolbert LM, Ozpineci B. Power cycle testing of power switches: A literature survey. IEEE Transactions on Power Electronics. 2014;**30**(5):2465-2473. DOI: 10.1109/TPEL.2014.2359015

[8] Shirani M, Aghajani A, Shabani S, Jamali J. A review on recent applications of brushless DC electric machines and their potential in energy saving. Energy Equipment and Systems. 2017;**3**(1):57-71. DOI: 10.22059/EES.2015.13911

[9] Held M, Jacob P, Nicoletti G, Scacco P, Poech MH. Fast power cycling test of IGBT modules in traction application. In: IEEE, editor. International Conference on Power Electronics and Drive Systems; May 26–29, 1997; Singapore, Singapore: IEEE; 1997. pp. 425-430. DOI: 10.1109/PEDS.1997.618742

[10] infineon. www.infineon.com. 1999–2018 [Updated: Aug 12, 2015]. Available from: https://www.infineon.com/dgdl/Infineon-AN2015_10_Thermal_equivalent_circuit_models-ANv01_00-EN.pdf?fileId=db3a30431a5c32f2011aa65358394dd2

[11] Luo H, Krueger M, Koenings T, Ding SX, Dominic S, Yang X. Real-time optimization of automatic control systems with application to BLDC motor test rig. IEEE Transactions on Industrial Electronics. 2017;**64**(5):4306-4314. DOI: 10.1109/TIE.2016.2577623

[12] Ma K, Vernica I, Blaabjerg F. Advanced design tools for the lifetime of power electronics-study case on motor drive application. In: Power Electronics and Motion Control Conference

(IPEMC-ECCE Asia), editors. 2016 IEEE 8th International; May 22-26, 2016; Hefei, China: IEEE; 2016. pp. 3255-3261. DOI: 10.1109/IPEMC.2016.7512816

[13] Melin P, Olivas F, Castillo O, Valdez F, Soria J, Valdez M. Optimal design of fuzzy classification systems using PSO with dynamic parameter adaptation through fuzzy logic. Expert Systems with Applications. 2013;**40**(8):3196-3206. DOI: 10.1016/j.eswa.2012.12.033

[14] National Instruments. www.ni.com. Introduction to Digital and Analog Co-Simulation between NI LabVIEW and NI Multisim [Internet]. 2013 [Updated: 2018]. Available from: http://www.ni.com/white-paper/13663/en/

[15] Nguyen V, Besanger Y, Tran Q, Nguyen T. On conceptual structuration and coupling methods of co-simulation frameworks in cyber-physical energy system validation. Energies. 2017;**10**(12):1-19. DOI: 10.3390/en10121977

[16] Parker MA, Soraghan C, Giles A. Comparison of power electronics lifetime between vertical- and horizontal-axis wind turbines. IET Renewable Power Generation. 2016;**10**(5):679-686. DOI: 10.1049/iet-rpg.2015.0352

[17] Pillay P, Krishnan R. Application characteristics of permanent magnet synchronous and brushless DC motors for servo drives. IEEE Transactions on Industry Applications. 1991; **27**(5):986-996. DOI: 10.1109/28.90357

[18] Poli R. Analysis of the publications on the applications of particle swarm optimisation. Journal of Artificial Evolution and Applications. 2008;**2008**(ID 685175):10. DOI: 10.1155/2008/685175

[19] Ponce CP, Ramirez FF, editors. Intelligent Control Systems with LabVIEW. 2010th ed. New York: Springer Verlag; 2010. 216p. DOI: 10.1007/987-1-84882-684-7

[20] Prabu MJ, Poongodi P, Premkumar K. Fuzzy supervised online coactive neuro-fuzzy inference system-based rotor position control of brushless DC motor. Institution of Engineering and Technology. 2016;**9**(11):2229-2239. DOI: 10.1049/iet-pel.2015.0919

[21] Premkumar K, Manikandan BV. Speed control of brushless DC motor using bat algorithm optimized adaptive neuro-fuzzy inference system. Applied Soft Computing. 2015;**32**:403-419. DOI: 10.1016/j.asoc.2015.04.014

[22] RENESAa. www.renesas.com. Semiconductor Reliability Handbook [Internet]. Jan.39.2017 [Updated: 2010–2018]. Available from: https://www.renesas.com/en-us/doc/products/others/r51zz0001ej0250.pdf

[23] Soulatiantork P, Alghassi A, Faifer M, Perinpanayagam S. IGBT thermal stress reduction using advance control strategy. In: The Scientific Committee of the 5th International Conference on Through-Life Engineering Services (TESConf 2016); December 2017; Vincent Building Cranfield University, UK. UK: Elsevier; 2017. pp. 274-279. DOI: 10.1016/j.procir.2016.09.040

[24] Vincotech. www.vincotech.com [Internet]. July 23, 2010. [Updated: June 23, 2017]. Available from: https://www.vincotech.com/search.html [Accessed: 10-0B066PA006SB-M992F09]

[25] Xia CL, editor. Permanent Magnet Brushless DC Motor Drives and Controls. 1st ed. Singapore: John Wiley & Sons Singapore Pte. Ltd.; 2012. 304p

[26] Zadeh LA. Fuzzy sets. Information and Control. 1965;**8**(3):338-353. DOI: 10.1016/S0019-9958(65)90241-X

[27] Zhang Y, Wang S, Ji G. A comprehensive survey on particle swarm optimization algorithm and its applications. Mathematical Problems in Engineering. 2015;**2015**:38. DOI: 10.1155/2015/931256

[28] National Instruments. www.zone.ni.com. IGBT Thermal Diode [Internet]. February 2017 [Updated: 2018]. Available from: http://zone.ni.com/reference/en-XX/help/375482B-01/TOC395.htm

[29] National Instruments. http://www.ni.com. Power Electronics Design with NI Multisim [Internet]. Jul 31, 2017 [Updated: Feb 21, 2018]. Available from: http://www.ni.com/white-paper/13714/en/

[30] Amin A, Hegazv OT. Swarm intelligence applications in electric machines. In: Lazinica A, editor. Particle Swarm Optimization. 1st ed. Rijeka: InTech; 2009. pp. 11-39. DOI: 10.5772/56679

[31] Bachache NK, Wen J. Multi objective swarm optimization design fuzzy controller to adjust speed of AC motor drive. In: Tan Y, Shi Y, Mo H, editors. 4th International Conference in Swarm Intelligence ICSI 2013. Harbin, China: Springer, Berlin, Heidelberg; 2013. pp. 522-529. DOI: 10.1007/978-3-642-38703-6_61

[32] Visconti P, Primiceri P. An overview on state-of-art and future application fields of BLDC motors: Design and characterization of a PC-interfaced driving and motion control system. ARPN Journal of Engineering and Applied Sciences. 2017;**12**(17):4913-4926

[33] Lai W, Chen M, Ran L, Xu S, Qin H, Alatise O, et al. Study on the lifetime characteristics of power modules under power cycling conditions. IET Power Electronics. 2016;**9**(5):1045-1052

[34] Abeyasekerab T, Rodriguez P. An overview of the reliability prediction related aspects of high power IGBTs in wind power applications. Microelectronics Reliability. 2011;**51**(9-11):1903-1907

[35] Choi UM, Blaabjerg F, Iannuzzo F. Advanced power cycler with intelligent monitoring strategy of IGBT module under test. Microelectronics Reliability. 2017;**76**:522-526

IntechOpen